Process Safety and Environmental Protection 135 (2020) 187–206

Contents lists available at ScienceDirect

Process Safety and Environmental Protection

journal homepage: www.elsevier.com/locate/psep

Experimental investigation of potential confined ignition sources for vapour cloud explosions

Jason Gill[a,b,*], Graham Atkinson[a], Edmund Cowpe[c], Herodotos Phylaktou[b], Gordon Andrews[b]

[a] Health and Safety Executive, Harpur Hill, Buxton, SK17 9JN, UK
[b] University of Leeds, Leeds, LS2 9JT, UK
[c] Health and Safety Executive, Redgrave Court, Merton Road, Bootle, L20 7HS, UK

ARTICLE INFO

Article history:
Received 21 October 2019
Received in revised form
20 December 2019
Accepted 21 December 2019
Available online 31 December 2019

Keywords:
VCE
Vapour cloud explosion
Vented explosion
Bang-box ignition
Nested ignition
Confined ignition sources
Buncefield

ABSTRACT

Electrical control boxes are common on high vapour cloud hazard sites, and in the case of the Buncefield explosion the ignition source was inside such a box, that was sited in an emergency pump house building. There has, however, been relatively little previous research into this type of ignition mechanism and its effect on the explosion severity. Commercially available electrical control boxes measuring 600 mm high, 400 mm wide and 250 mm deep were used to explore the pressure development, venting processes and flame characteristics of stoichiometric propane/air explosions using aluminium foil and the supplied doors as vent coverings. In some tests, the boxes were empty in order to establish a baseline for the effect of the internal congestion of the boxes. In other tests a congestion array was added. It was found that, in both the empty and congested box tests, the door produced a flat petal shaped flame, which differed drastically from the mushroom flame shape and associated rolling vortex bubble venting that is traditionally observed with large orifice vented explosions.

1. Introduction

The most recent severe Vapour Cloud Explosion (VCE) in the United Kingdom was the Buncefield incident in 2005 (Major Incident Investigation Board, 2007). The vapour cloud was caused by a release of winter grade gasoline at a rate of around 120 kg/s that continued for 1380 s, in zero wind conditions. This resulted in a large unconfined, gravity driven pancake cloud and the resulting explosion was severe.

A recent review (Atkinson et al., 2017a) into the cloud formation at VCE events at large fuel storage sites has shown that many of these events are similar to Buncefield in that they were relatively slow releases, i.e. not catastrophic failures, that have occurred at times when weather conditions allow the formation and persistence of a pancake type cloud. The clouds accumulated for several tens of minutes and in some cases over an hour before ignition occurred.

The idea of very large homogenous cloud development (Atkinson and Coldrick, 2012; Atkinson et al., 2015; Coldrick et al., 2011) is relatively new and not widely understood. Away from the immediate vicinity of the leak the movement of hydrocarbons from a leak in very low wind speed conditions is driven by gravity. This form of vapour transport is very different from wind dispersed plumes. The vapours spread in all directions from source in a flow that laminarises in the contact layer with overlying fresh (lighter) air Briggs et al. (1990). This means that the flow can travel for many hundreds of metres without dilution, potentially leading to near stoichiometric concentrations over almost the entire footprint of the cloud.

Atkinson et al. (2017b) concluded that eventual ignition of this type vapour cloud is a much more likely outcome than for dispersion occurring in windy conditions; primarily because the cloud size for a given source is typically hundreds of times larger. The cloud is also present for sufficient time to ingress into confined spaces containing ignition sources (that may be well away from the source) before it is dispersed by a change of weather conditions.

The ignition source for the Buncefield explosion was within an electrical control box, situated inside an emergency pump house (Atkinson, 2006) where it was submerged in the vapour cloud for a high proportion of the total release time. This control box held a

* Corresponding author at: Health and Safety Executive, Harpur Hill, Buxton, SK17 9JN, UK.
E-mail address: jason.gill@hse.gov.uk (J. Gill).

https://doi.org/10.1016/j.psep.2019.12.026

Nomenclature

t	Time after ignition
M	Mass of unburned gas in the box
V	Volume occupied by unburned gas in the box
H	Height of the box
W	Width of the box
ρ	Density (of the unburned gas)
ρ_0	Initial density (of the unburned gas)
P	Pressure (of the unburned gas)
P_0	Initial pressure
A_{door}	Area of door opening
A_{vent}	Effective area of vent (at the vena contracta)
C_d	Discharge coefficient
I	Moment of inertia of door and catch about hinges
θ	Angle of the door to the closed position
E	Expansion ratio
V_b	Burning velocity
R	Flame radius
C	Speed of sound
a	Linear acceleration of a detached panel
Δv	change in speed of a detached panel
L	Height of a building

star-delta starter, designed to supply a large three-phase motor, the fire pump, with a reduced voltage of 230 v in star configeration during start up. Once the motor has reach a set speed, contactors in the starter engage to change the supply configuration to the the motor to delta, supplying 415 v. It is likely that a spark caused during the contactors opening or closing was the ignition source.

In the event of large persistent homogenous clouds on other sites there is a fairly high probability that the final ignition source will be of this sort i.e. within a cabinet or box which is in itself located in a larger structure engulfed by the cloud. Some control boxes are supplied as gas tight, but entry points need to be made to allow for cabling and connections etc. The boxes are generally mild steel and may also suffer degradation and seals may perish over time affecting the gas tightness. It is possible to mitigate against the production of sparks in the design and manufacture of control boxes, making them intrinsically safe, but this is an expensive process and is usually reserved for zoned areas. As highlighted by Atkinson et al. (2017a) in most of these events the clouds have extended over large areas beyond zoned areas.

There has been a lot of discussion regarding the mechanisms that contributed to the severity of the explosion. Much of this has been focused on the effects of congestion; recent tests have shown that it is possible to have a high-order explosion in an unconfined cloud if there is significant congestion (Pekalski et al., 2015). But there is a potential that this multi-compartment confined ignition source, in essence a 'nested bang-box', may have been a contributing factor (Gill et al., 2019). There has, however, been little in the way of research into the effects of such bang-box ignition sources on the severity of VCEs, despite the need for such work being identified some years ago (Bradley et al., 2012).

Buncefield is not an isolated historical case in terms of ignitions occurring within nested confined enclosures. The severe explosion at Port Hudson (Burgess and Zabetakis, 1973) is believed to have started within a freezer located within a concrete building that was submerged in an LPG cloud.

The primary ignition at the San Juan VCE in 2009 was also within an electrical control cabinet. However this was not nested in a larger building and the gasoline vapour cloud around the point of ignition was shallow. Ignition in this case resulted in a slow flash fire; transition to severe explosion occurred later in the event.

Fig. 1. Test rig with electrical control box in place.

Fig. 2. Control box door showing three point locking mechanism.

There has been considerable useful research available on vented explosions from vessels and much is known on this subject. During the internal explosion in a vessel the pressure builds until the point of vent failure. Once there is a vent, unburnt gas will be pushed out by the internal flame; this can be as much as 80 % of the total vessel volume. Once the flame exits the vessel this will ignite any vented flammable gas not diluted by the atmosphere in its wake. The external explosion is often more severe than the internal explosion and there are many factors that can contribute to the severity, such as vent size (Bauwens et al., 2010) and vent burst pressure (Fakandu et al., 2015). The internal gas concentration before ignition can have an effect; rich mixtures often result in more severe

Fig. 3. Chassis plate used to add congestion.

Fig. 4. Congestion array fitted inside box.

Table 1
Results of overpressure measurements for tests.1–5.

Test	Vent covering	Congestion	PT1 (mbar)	PT2 (mbar)	PT3 (mbar)
1	Foil	No	97	5	5
2	Foil	No	68	3	3
3	Door	No	86	Failed	8
4	Door	No	90	4	7
5	Foil	Yes	109	17	9
6	Foil	Yes	131	20	17
7	Door	Yes	312	Failed	56
8	Door	Yes	289	16	41
9	Door	Yes	351	24	59

explosions as there is more fuel available for combustion (Gill et al., 2016) and the opposite is true of lean mixtures. Vessel length and internal congestion can have a significant escalating effect (Tomlin et al., 2015). Both of these allow flame acceleration within the vessel which increases the outflow speed of the unburnt gas generating more turbulence within this unburnt gas cloud. Although if the turbulence is high there is a possibility that much of the unburnt gas could have been diluted below the flammable limit by the shear mixing with the atmosphere caused by the turbulent outflow.

When an explosion propagates from a vessel into a flammable cloud the external explosion becomes the ignition source for the external cloud and a large ignition source can increase the severity of an explosion. This effect has been used many times to give a 'head start' to unconfined vapour cloud explosion experiments. If the vessel is sufficiently large and the venting is into significant congestion, transition to detonation can occur (Harris and Wickens, 1989).

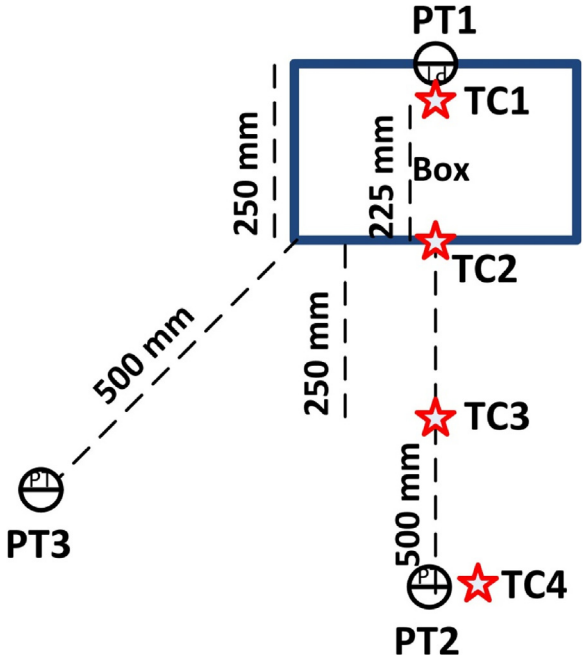

Fig. 5. Plan view of location of pressure transducers (PT) and thermocouples (TC).

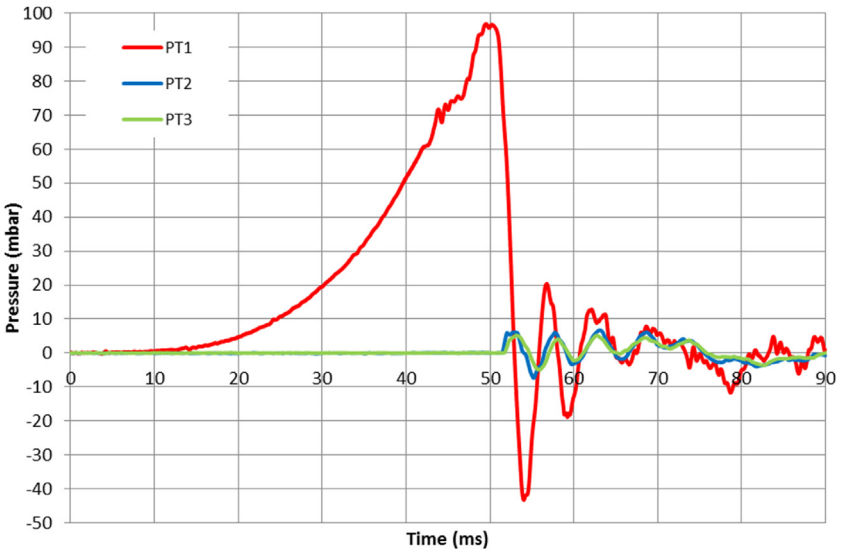

Fig. 6. Pressure trace for Test 1.

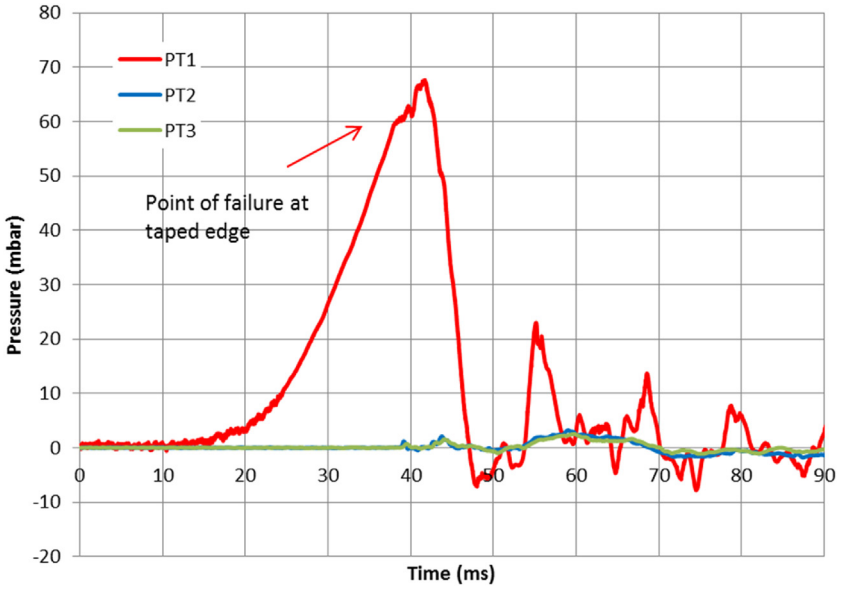

Fig. 7. Pressure trace for Test 2.

Table 2
Maximum rate of pressure rise within the boxes.

Test	Vent covering	Congestion	Max pressure at PT1 (mbar)	Max pressure rise rate at PT1 (mbar/ms)
1	Foil	No	97	5.8
4	Door	No	90	4.6
6	Foil	Yes	131	20
9	Door	Yes	351	44.8

Recent research into the propagation of a confined explosion to an external cloud by Daubech et al. (2017) was conducted to look at the effects of the Buncefield type ignition process. They used a 4 m^3 vessel to propagate an explosion into a 54 m^3 'unconfined' flammable volume. Two vent sizes were compared, 0.5 m^2 and 0.04 m^2. They concluded that there was little interaction between the venting flame and external volume with the large vent because the discharging gases assumed the shape of a rolling vortex bubble which did not break down before it was ignited by the exiting flame. With the smaller vent area the venting gases from the confined space formed a jet before it was ignited by the exiting flame, which then travelled rapidly through the jet. In this instance the severity of the explosion in the external cloud was increased compared to the larger vent. Modelling conducted during the study showed that the jet generated high levels of turbulence and entrained the external volume and there was little entrainment with the rolling vortices generated with the larger vent. This research, however, did not take into account the hinged-door confinement of typical equipment cabinets and the effect this has on venting and flame propagation.

This paper describes experimental results comparing the effect on flame shape of venting from a hinged door with that from a bursting membrane vent cover, often used in vented explosion experiments. This work forms the initial stages of a larger programme of work, which will investigate the propagation of a congested and confined explosion from a hinged door electrical control box into an external flammable volume.

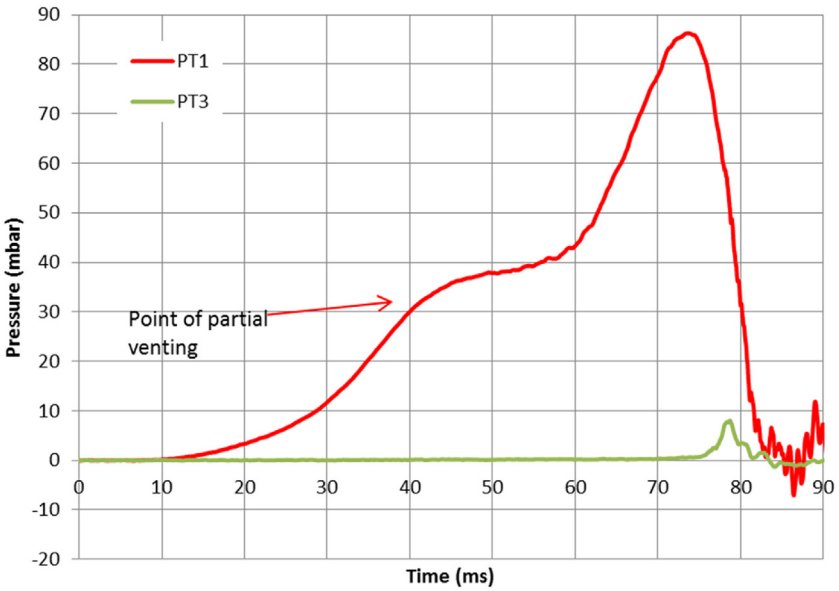

Fig. 8. Pressure trace for Test 3.

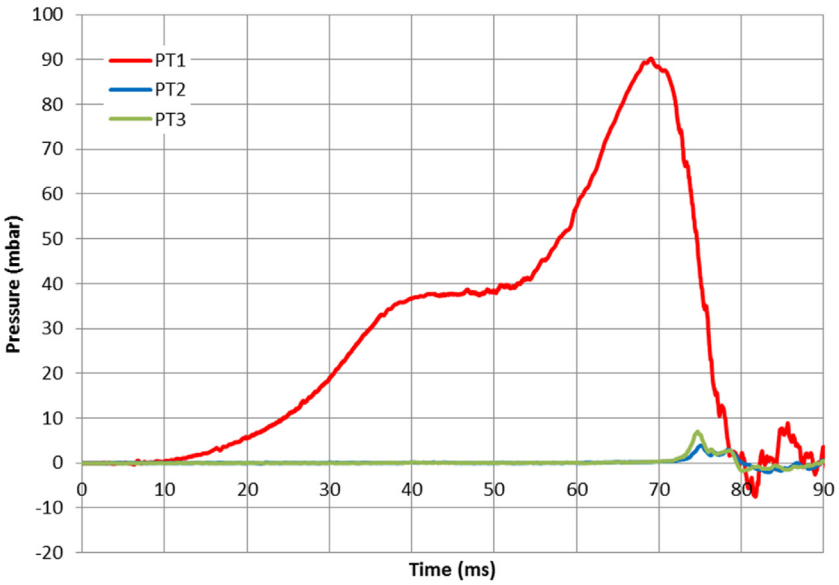

Fig. 9. Pressure trace for Test 4.

2. Methodology

Commercially available electrical control boxes 600 mm high, 400 mm wide and 250 mm deep, volume 0.06 m^3, were fitted to the back wall of a 8 m^3 frame rig as shown in Fig. 1. The boxes have a full steel door with a mass of 3.29 kg, as shown in Fig. 2. The door is attached by two 50 mm long hinges. The door has a soft foam rubber gasket that fits around the lipped flange of the box. The closing mechanism is a 15 mm wide plastic catch that engages with the inside of the flange on the longest wall when the removable external handle is rotated. Protruding from the catch are two 5 mm diameter steel bars that engage with the inside of the flange at the top and bottom; these are stabilised near the door with weak plastic supports. The shape of the flange leaves an actual opening of 365 × 560 mm. The entire closing mechanism is designed to be easily removed by the user to allow for the replacement of the handle with an aftermarket key locking handle. The door and hinges are designed to be easily removed and inverted by user. During these tests, the door and hinge pin were replaced with new ones after each test. For four of the tests the door was removed completely and the opening was covered with an aluminium foil membrane: this foil produces comparable bursting pressures to the door (Gill et al., 2019). Due to the shape of the orifice, designed to seal on the door, the foil had to be taped to the flat surfaces of the box with duct tape. The left side wall of one of these boxes was cut away and replaced with 5 mm polycarbonate sheet for viewing purposes.

Control boxes are usually full of equipment which will act as congestion elements. The contents of these boxes are highly varied depending on their use. There may be large and small electrical components, cabling and pneumatic tubing. The boxes are also available in a wide range of sizes and styles. Generally the economic driver will be to utilise the space within the smallest possible box for the required task.

To limit variables only one style and size of box was used for testing. For tests in which congestion was added the aim was not

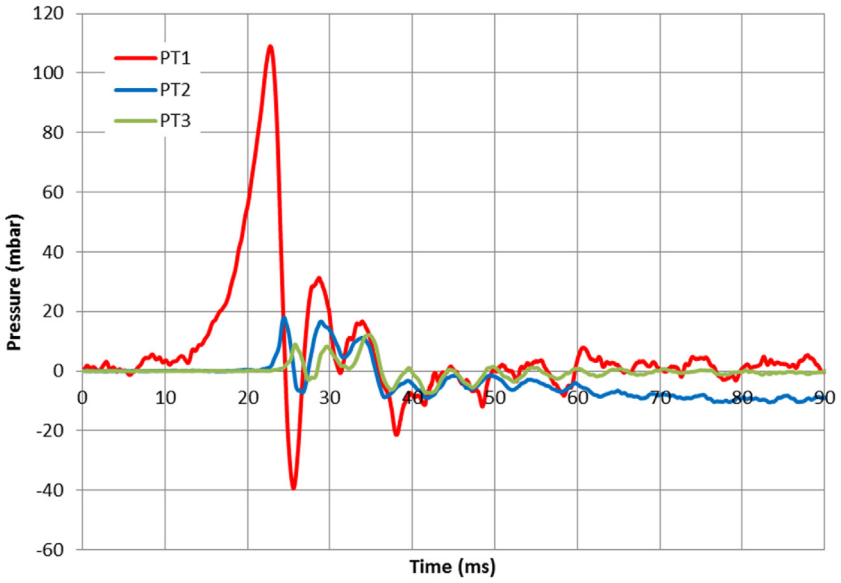

Fig. 10. Pressure trace for Test 5.

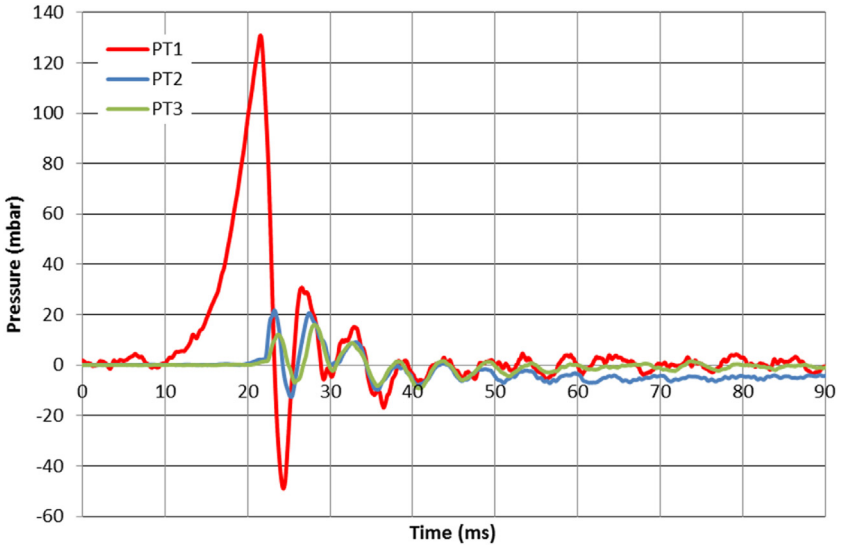

Fig. 11. Pressure trace for Test 6.

Table 3
Measured flame arrival times and average flame speeds between thermocouples.

Test	Vent covering	Congestion	TC2 (ms)	Average flame speed (m/s)	TC3 (ms)	Average flame Speed (m/s)	TC4(ms)	Average flame Speed (m/s)
1	foil	No	51	4.41	65	17.86	81	15.65
2	Foil	No	44	5.11	69	10	88	13.15
4	door	No	53	4.25	–	–	–	–
6	Foil	Yes	28	8.26	36	31.25	42	20.833
8	Door	Yes	30	7.5	–	–	–	–
9	Door	Yes	30	7.5	–	–	–	–

to recreate a specific installation but to produce a configuration that was robust, easily reproducible and consistent between tests. Commercially available chassis plates were used, shown in Fig. 3, designed to fit inside the box and be used to attach equipment. Four of these chassis plates were bolted together with a spacing of 50 mm and attached to the inside of the box with the intended mounting bolts. The grid has a blockage ratio of 21.5 % in the centre with a solid border around the edges and mounting points. When fitted there is a 25 mm gap around the plate as shown in Fig. 4. The mounting points of the forward three grids were cut away to facilitate fitting of array as a single piece. In testing the flame travels through the central gridded section before vent failure and this changes the combustion mechanics.

Tests were conducted using stoichiometric propane/air mixtures (4.2 %) ignited by a Talon^{TM} tungsten hot wire ignitor at the centre of the back wall of the box. The ignitor is non-pyrotechnical, it provides a hot surface for ignition without adding significant energy or turbulence to the ignition event. The gas concentration

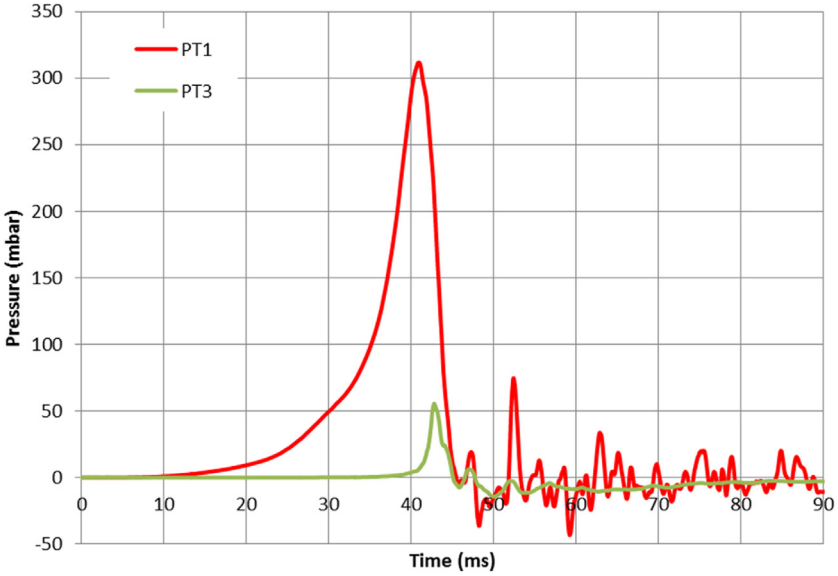

Fig. 12. Pressure trace for Test 7.

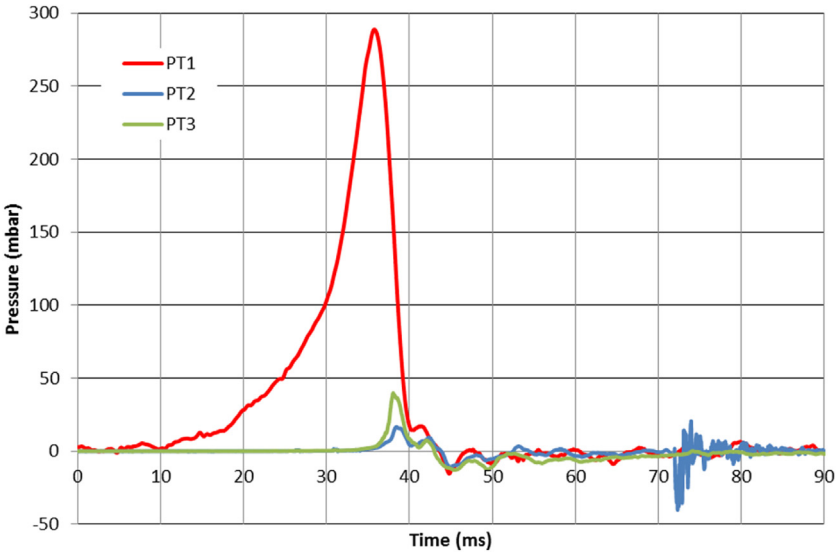

Fig. 13. Pressure trace for Test 8.

was controlled with mass flow controllers. The box was filled by purging the box with pre-mixed gas at the desired concentration and monitoring the exhaust with a gas analyser to ensure purging was complete.

Overpressure measurements were made using fast response pressure transducers, which were located both inside and outside the box, as shown in Fig. 5. Fast response thermocouples were place internally and externally at set distances to record flame arrival times. All the tests were filmed at 240 frames per second (fps), with the exception of Tests 7 and 9 where the recording failed. Tests 6 and 8 were filmed at 1000 fps from the side and 240 fps from the front.

3. Results and discussion

Nine tests were conducted, five with a door and four with foil covering the opening. Three tests with doors and two tests with foil had the congestion elements added. The overpressures and flame characteristics were recorded.

3.1. Pressure development

Examples of the pressure development are shown in Figs. 6–14. The overpressures recorded during each the tests are detailed in Table 1. The results, on face value, show similarities in the maximum pressures between the uncongested foil tests (Fig. 6) and door vent coverings tests (Fig. 9). The bursting pressure was dominant in these tests and any external explosion was inconsequential.

With the addition of congestion there is a drastic increase in the speed of the pressure rise compared to the uncongested tests in the case of both foil (Fig. 11) and door (Fig. 14) vent coverings (Table 2). The maximum pressure was reached in one third of the time with the addition of the congestion. The congested tests show an increase in maximum internal overpressures. There was a substantial difference in these overpressures between the congested door and congested foil tests.

With the addition of congestion the external overpressures recorded were also higher, both in absolute values and as a fraction of the peak internal pressure compared to the uncongested

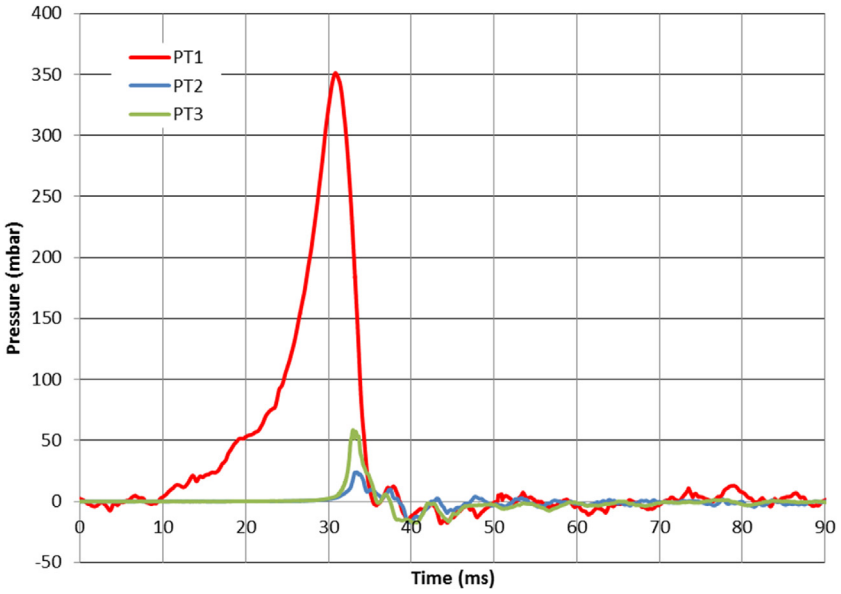

Fig. 14. Pressure trace for Test 9.

tests. Even with congestion, the external pressures were still very low.

It is evident from the pressure traces (Fig. 9) and analysis of video that in the uncongested tests using the door (Tests 3 and 4) there was a momentary pause in pressure rise due to the effect of venting. This is due to the pressure rise causing deflection in the door, which breaches the gas tight seal made by the door. The pressure then continues to rise until the door catches are overcome and the door is pushed open. In the foil tests the foil remains gas tight until it bursts or tears. This effect is still evident with the addition of congestion (Fig. 14), but is less pronounced. This may be due to the increase speed of the pressure rise overcoming the catches before substantial elastic deformation of the door can occur.

It proved difficult to provide a reproducible foil seal for these commercially available boxes. Of the two uncongested foil tests Test 1 gave higher maximum pressure as the foil was pushed very tight and tore around the centre of the orifice. In Test 2 the foil started to breach near the taped seals at the edge of the orifice. In this case the results may not be representative of the bursting pressure of the foil as venting may will have occurred as the tape detached (Fig. 7). Similar variability was observed in congested tests with foil: Test 6 gave higher maximum pressure as the foil tore close to the centre of the orifice, whilst in Test 5 initial failure around the taped edge, again, led to lower pressures.

Venting by the door generally appeared more reproducible. The increase in pressure in Test 9 compared with Tests 7 and 8 is because in the later experiment a new, solid box, with no viewing window cut out was used. This makes the box stiffer on the side where the door catches engage and delays venting.

3.2. Venting

Given the large vent area relative to the volume of the box, it could be expected that if the vent closure was fairly weak then the peak pressure would be dominated by the external part of explosion (Proust and Leprette, 2010). In this case, however, the burst pressure is dominant, an effect also observed by Fakandu et al. (2015).

In the case of the foil, the burst pressure is relatively high, but once a crack is initiated it propagates rapidly and a large vent area is created within a few milliseconds. Internal pressure and outflow velocities decline immediately, and there is no extended period of high speed jetting through a small opening. There is relatively little difference in the maximum pressure in congested and uncongested tests because the rapidly widening vent allows efficient venting immediately.

The resulting outflow of gas has a broad central core in which the flow is irrotational and largely unaffected by the vorticity in the shear layers at the edge. This type of flow has been described as a "rolling vortex bubble" Maxworthy (1972); Daubech et al. (2017). As these layers roll up, the potential core of the resulting vortex is eroded slowly by relatively low levels of shear, resulting in slow combustion and low external overpressures.

In the uncongested door tests, venting commenced at lower pressures (40 mbar) as the door begins to deflect, and this venting initially offsets the rate of pressure rise. There is then an extended period (~20 ms) in which gas is forced out of the resulting crack at a speed of around 80 m/s. Eventually, increasing levels of volume production associated with the developing flame cannot be offset by venting through the crack associated with flexure of the door and the pressure begins to rise again. The internal pressure and outflow velocity increase to 90 mbar and 120 m/s respectively. The final pressure at which the catch fails is comparable with the foil, but even when the catch has failed the inertia of the door restricts the rate of opening. The rate of depressurisation is, therefore, relatively slow, and there is a significant period (of order 10 ms) in which the jet outflow continues. By the time the flame exits the door is open by no more than 30 mm and the pressure and vent flow speed have declined.

In the case of the congested door test the pressure rise occurs more quickly. The inertia of the door means that even after the catch fails there is a substantial increase in pressure before the open area has grown sufficiently to control the pressure rise. The final pressure of 350 mbar corresponds to an outflow speed of around 230 m/s (Fig. 15). The maximum pressure rise rates within the boxes for the four test types that achieved the highest over pressure are detailed in Table 3.

The ejected gas in the door tests formed a narrow, high-speed jet. Only a very small proportion of the gas remains in the irrotational potential core of the jet and most of the ejected gas is immediately entrained into the turbulent shear layer where high flame speeds could develop. In these initial experiments, the box is surrounded by air, so entrainment also leads to rapid dilution of the

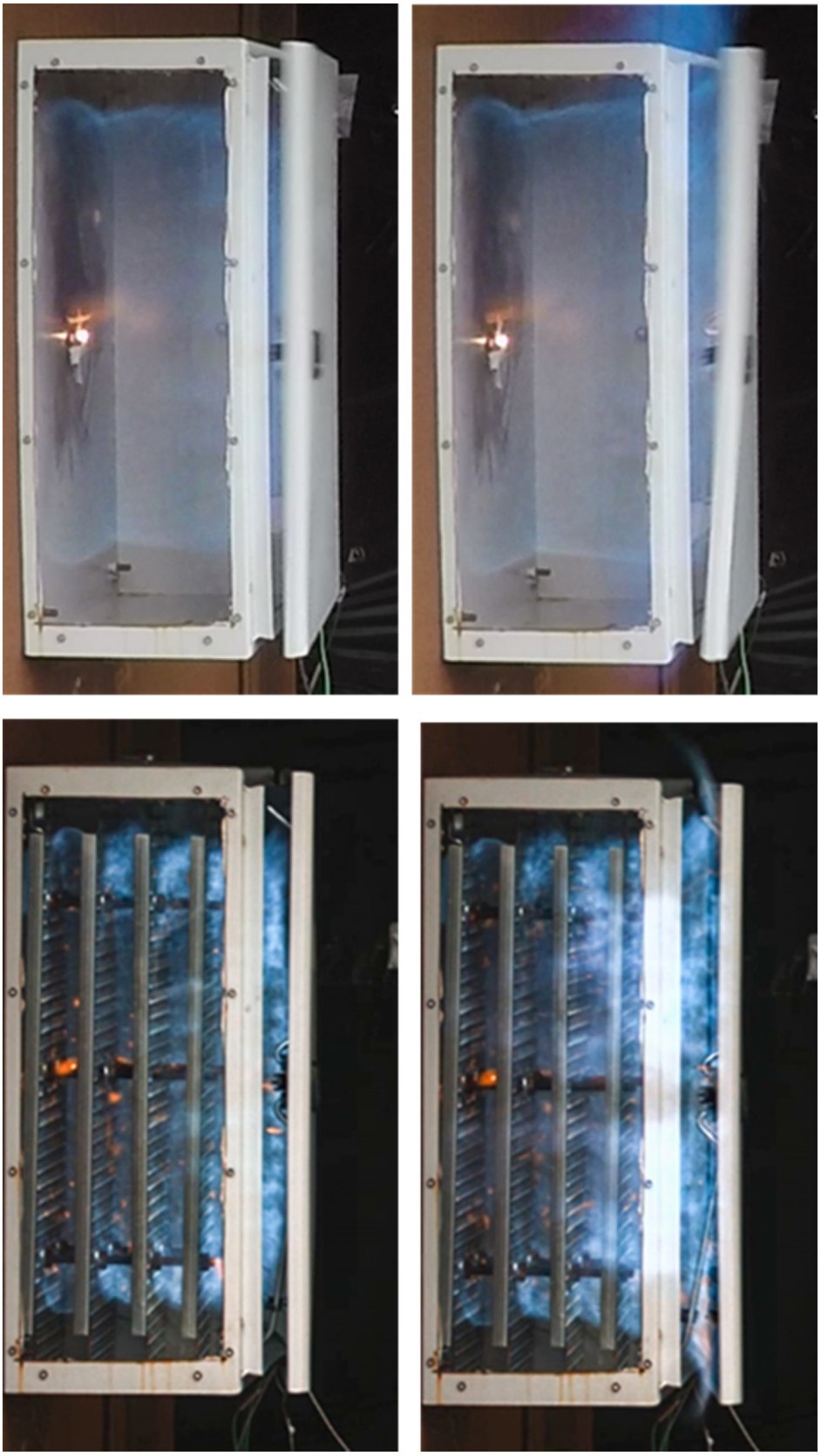

Fig. 15. Video stills showing the opening position of the door during the final stages of venting and flame exit, the frame intervals are 4.17 ms for uncongested (top) and 1 ms for congested (note slight angle of view difference).

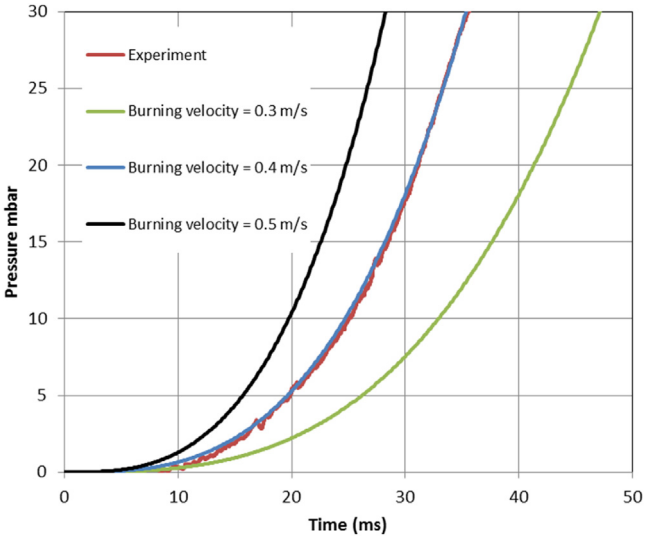

Fig. 16. Modelling of the early stages of pressurization.

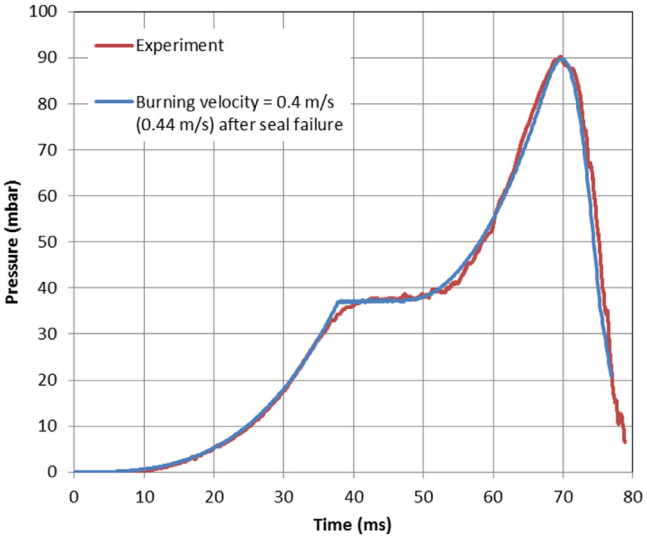

Fig. 17. Modelling of pressurisation and venting with a fixed burning velocity.

pre-mixed gas below the initial (stoichiometric) concentration; this limits the rate of burning and overpressure when the flame arrives. This would not be the case if the atmosphere outside the box was also flammable.

3.3. Modelling of pressurisation and venting

Video images after ignition show a growing hemispherical flame shape and it is possible to predict the rate of pressure rise for a given flame speed using the Bernoulli (Energy) Equation in the incompressible limit. The flame speeds are so low that the pressure will rise uniformly throughout the box. The venting pressures are so low that the box is sufficiently rigid that changes in its volume prior to venting are negligible.

The later pressurisation and venting can also be modelled. Assumptions have to be made about the pressure at which the rubber seal is breached and the effective size of the resulting vent A_{vent}. The pressure at which the door catches fail also has to be taken from experiment but the opening of the door can be calculated given the moment of inertia about the hinge and internal pressure.

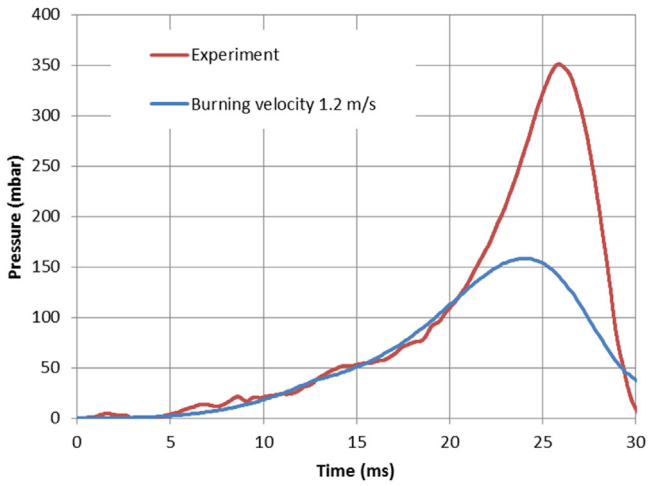

Fig. 18. Pressurisation in box with congestion.

The equation for the expanding radius of the flame R is

$$\frac{dR}{dt} = V_b E$$

Where V_b is the burning velocity and E is the expansion ratio

Generally the burning rate was assumed to be constant but in some cases the effect of a small change in the burning velocity after venting were investigated.

The equation for the mass of unburned gas within the box is as follows.

$$\frac{dM}{dt} = -\rho V_b 2\pi R^2 - \rho A_{vent}\sqrt{\frac{2P}{\rho}} - \rho C_d A_{door}\sqrt{\frac{2P}{\rho}}$$

A_{vent} the effective area of the vent at the vena contracta, has to be taken from the experiment. The discharge coefficient, C_d, for the door is assumed to be 0.6.

The equation for the volume of unburned gas within the box is as follows

$$\frac{dV}{dt} = -EV_b 2\pi R^2 + \frac{HW^2}{2}\frac{d\theta}{dt}$$

The change in pressure of the unburned gas is calculated from the change in density

$$P = P_0 \frac{M}{V\rho_0}$$

The area of the door vent is

$$A_{door} = HW\theta + W^2\theta$$

The equation of motion of the door is

$$\frac{d^2\theta}{dt^2} = \frac{PHW}{2I}$$

Fig. 16 shows the predicted rates of early pressure rise for a range of burning velocities. In all cases it is assumed that the expansion ratio is 7. The results show that the effective burning velocity is very close to 0.40 m/s and the flame speed (where the burned gas is stationary) is $0.4 \times 7 = 2.8$ m/s.

Results for the later stages of a typical uncongested test are shown in Fig. 17.

A small increase in flame speed occurred in the latter stages before venting. Fig. 18 shows the effect of increasing burning velocity by 10 % after the point when the seal failed and the resulting internal flow began. This change in flame speed appears to roughly account for the observed increase in pressurisation.

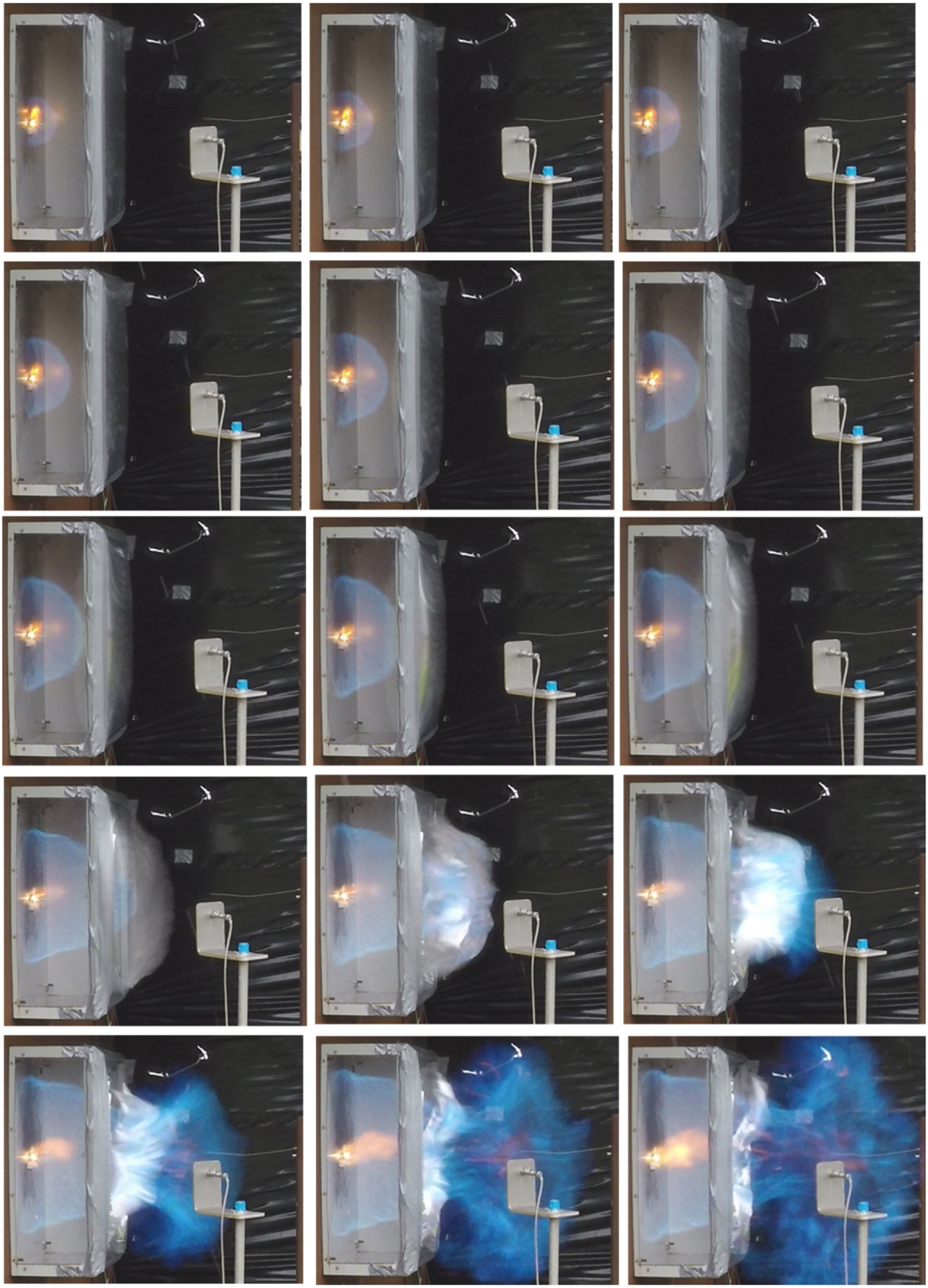

Fig. 19. Flame development in Test 1; frame intervals 4.17 ms.

When there was congestion the rate of pressurisation was higher. Again the videos show that, until the door fails, the flame is roughly hemispherical, so a simple model of combustion rate is possible. In this case the initial average burning velocity was around 1.2 m/s (flame speed 8.4 m/s). There was a marked increase in the burning rate after the door started to open at around 80 mbar. This was presumably traceable to the onset of flow towards the vent which drove unburned gas through the congestion array, increasing turbulence levels and consequently flame speeds. The hemispherical symmetry of the flame would have been broken down after this

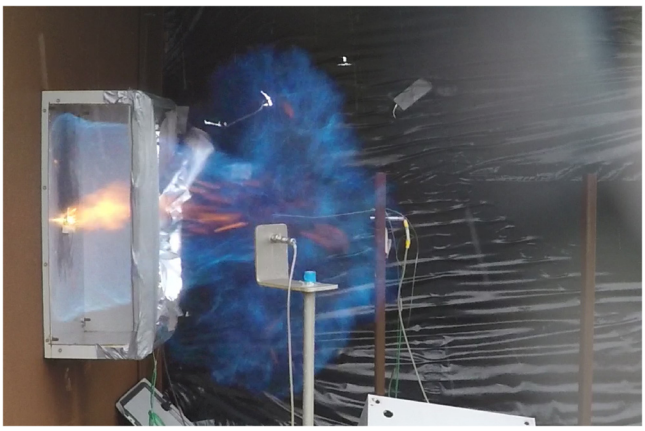

Fig. 20. Test 1 – initial mushroom flame, typical of rolling vortex bubble venting.

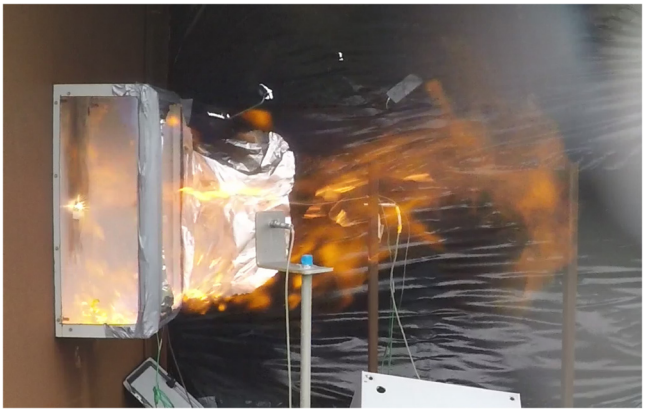

Fig. 21. Test 1 - secondary mushroom flame, typical of rolling vortex bubble venting.

point and the burning velocity could not adequately be represented by a single value.

As with these calculations the vent are has been assumed further experimental work is required to measure the true vent area as a function of time during these event.

3.4. *Flame characteristics and measured flame speeds*

In the foil tests (Fig. 19), the flame develops near hemispherically towards the front of the box from the initial kernel, with some distortion and elongation caused by the back wall of the box. The foil is pushed forward and taut before tearing vertically, and as the flame exits it burns through the vented gas and establishes a typical mushroom shape (Fig. 20). This shape is characteristic of the vented gases forming a rolling Maxworthy vortex bubble. As the flame extends, it forms a second mushroom shape (Fig 21), which reinforces the theory that the rolling vortex bubble method of venting applies in this case (Fig. 16). The flame extends to near the edge of the 2 m long rig. In Test 2 the measured average flame speed to TC2 is higher; this is likely a factor of the early failure of the foil at the taped edge causing venting and therefore disrupting the internal flame development.

In the door tests (Fig. 22), the flame inside the box develops in a similar manner to that in the foil tests. However, the door starts to deflect before the flame has reached a diameter of 200 mm, due to yielding of the locking bar mechanism. As the pressure builds, either one or both of the locking bars fail, which facilitates door opening. The door is open by no more than 30 mm when the flame begins to exit, and combustion is complete before the door is completely open. The pattern of the event is the same with the addition of congestion; it is just a faster event (Fig. 23). The external flame does not develop into a mushroom shape, but is initially a flat petal shape which expands sideward and in the direction of the door for approximately 1 m (Fig. 24). Flame arrival times (relative to arrival at TC1) derived from the thermocouple measurements are shown in Table 3. Failure of door catch occurs slightly before the flame arrival at TC2 and the induced flow of unburned gas means that even within the box the observed flame speeds are not simply related to the underlying burning velocity – although they are similar. Likewise in the foil tests without congestion the vent burst before the arrival of the flame at TC2 distorting the measured average flame speed.

For the foil tests the flame impinged on TC3 and TC4, well outside the box. Movement of unburned gas in the jet forced out of the developing split in the foil accounts for most of the of the observed flame movement and the arrival times give an indication of the velocity of unburned gas.

Due to the venting location with the door on, the flame does not reach the external thermocouples; further work to measure the external flame speeds by this method is planned for the future.

The video records of tests with the door allow an alternative method of assessment of the rate of progress of the flame outside the box. The video from the front of Test 8 (Fig. 24) was captured at a rate of 240 frames per second giving an interval of 4.17 ms between frames. In the first frame that flame is seen external to the box it has travelled 250 mm. Using the side view (Fig. 25) with a higher frame rate to estimate the time of emergence prior to this image, gives a flame speed of approximately 200 m/s. Most of this speed is movement of unburned gas in the jet from the door. The measured pressure at the time of emergence of the flame was around 290 mbar which also corresponds to an expanded gas velocity of around 200 m/s.

The flame travels a further 300 mm in the next 4.17 ms frame interval (an average of 72 m/s) and a further 100 mm in the next frame (24 m/s). These result confirm the expected increase in the velocity of the unburned gas flow where venting is through a door rather than foil.

As previously discussed, given the vent geometry and high venting velocities indicated by the flame speeds it would be expected that the sheer turbulence would be very high, causing dilution with the entrained air. Using the video the external flame before it starts to dilute, in Test 6, the flame was a rough mushroom shape around 1000 mm in diameter (Figs. 26 and 27). In Test 8 the flame is a rough petal shape, approximately $800 \times 600 \times 150$ mm at its extremes before the flame dilutes (Figs. 24 and 28). Although the shapes are very different it is clear that the door produces a much smaller flame than the foil.

If the flame shape for the foil test is simplified to a hemisphere and the size calculated using the expanded gas volume, the theoretical maximum diameter of the flame is around 1200 mm. This is very close to the observed flame size. This suggests that most of the gas burned and only a small proportion was diluted below the LFL.

Conversely if the door flame shape is simplified to a disk of width 150 mm, the expected flame diameter would be around 1900 mm which is much larger that the reach of the flame observed (800 mm): this suggests that a high proportion of the ejected gas was diluted to the point where it did not burn.

4. Conclusions

Within the box the flame develops hemispherically in a predictable manner at a laminar burning velocity of approximately 0.4 m/s, leading to a predictable rate of pressure increases. The addition of an internal congestion array increases the burning velocity

Fig. 22. Flame development in Test 4; frame intervals 4.17 ms.

Fig. 23. Flame development in Test 8: frame interval 1 ms.

Fig. 24. Front view of venting flame shape in Test 8; frame interval 4.17 ms.

threefold but the flame still develops as a hemisphere and pressure development is still predictable. The flame becomes more turbulent and asymmetric once the vent fails and unburned gas starts to flow towards the opening. The resulting increase in flame speed is difficult to predict.

Without congestion there is approximate correspondence between the door and foil in terms of internal flame speeds and burst pressure. The highest pressures occur just before the start of venting. The addition of congestion removes this correlation between the internal peak pressure and the vent opening and

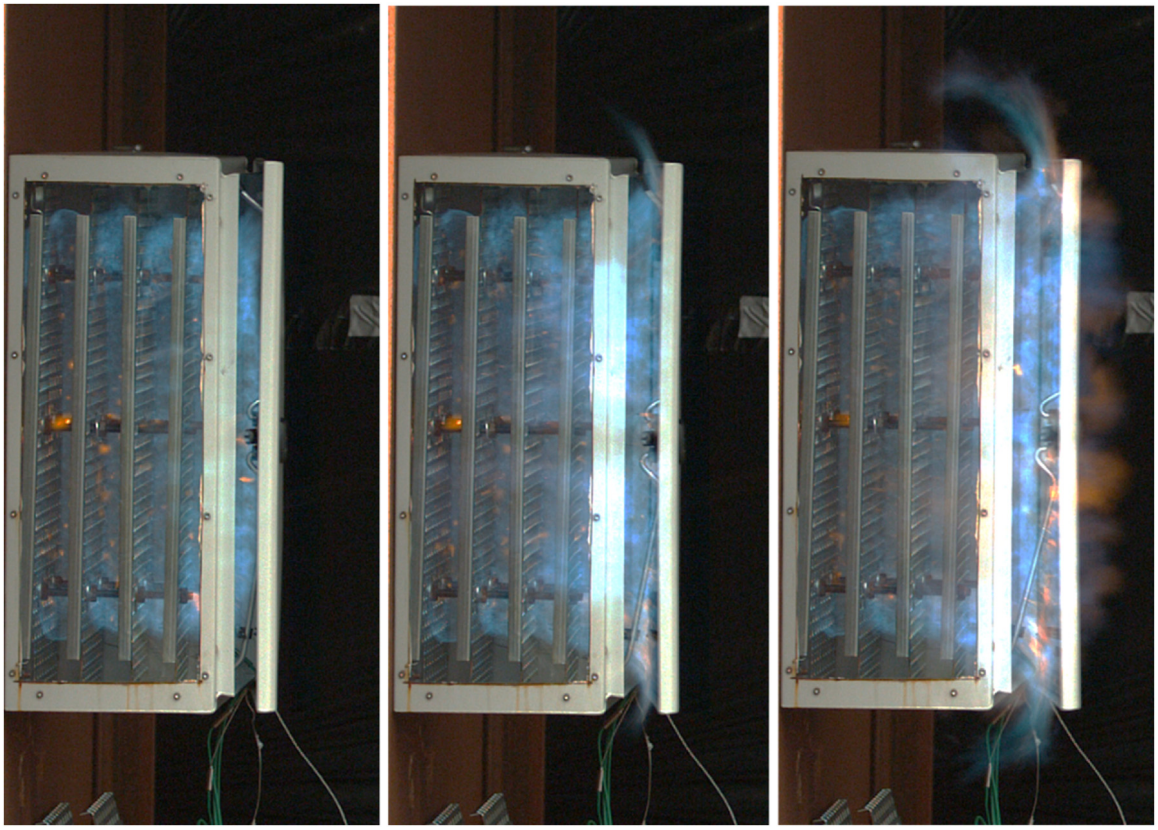

Fig. 25. Side view of Test 8; frame interval 1ms.

there are substantial differences in internal pressure measurement between the two types of closure. In the foil and congestion tests the maximum achieved overpressure was 131 mbar; in the door test the maximum overpressure achieved with congestion was 351 mbar. These differences arise because of differences in the effective inertia of the foil and door. The foil is very light and removed quickly from the vent area once torn. The door has substantial inertia, so moves relatively slowly and continues to restrict venting well after the catch fails. If the pressure is rising rapidly because of congestion then the relatively slow opening of the vent leads to higher pressures.

The foil tears rapidly, so the venting process happens almost instantaneously and the unburnt gas forms a rolling vortex bubble. This bubble entrains little of the external atmosphere, which in these tests is air. The flame propagates through the unburnt gas bubble before it has chance to break down, producing the typical mushroom cloud. This means that the size and shape of the flame is predictable as little of the gas is lost due to dilution through entrainment of air. Most of the released gas burns before it is diluted below the flammable limit. However the limited mixing at the edge of the vortex bubble implies that the rate of associate flame acceleration is also low. The external flame still provides a large ignition source for an external volume which is likely to have an escalating effect.

The door has a large surface area and has substantial mass in comparison to the foil; the doors under test have a mass of 3.2 kg. The door is fixed to the 1860 mm circumference of the door frame at five points by two 50 mm long hinges, two 5 mm diameter bars and a 15 mm wide plastic catch. It appears that as the pressure rises the door flexes allowing venting to start through the small gap created by the movement. Even when the pressure overcomes the door catch and locking bar, inertia means the door is still causing a considerable blockage. The venting gas is forced out of the thin wedge shape vent, caused by the slightly open door. In the empty box tests the venting gas stream reaches speed of 120 m/s but with the addition of congestion this increases to a maximum of 230 m/s in these tests. This venting gas stream has a high speed and large surface area, maximising the potential for shear generated turbulence.

In these tests this rapid mixing with external air causes dilution below the flammable limit for a high proportion of the unburned gas driven out of the box. The door is open by no more than 30 mm at its widest point when the flame exits. The flame accelerates axially to close to the venting gas velocity as it ignites the vented gas, rapidly slowing as it enters the cold atmosphere. The resultant fireball is much smaller than that of the foil tests due to the mass loss of available fuel via the dilution caused by entrainment of air into the gas stream.

If these tests were conducted with a flammable external volume the different venting mechanisms would have more significance. The foil burst venting mechanism generates little turbulence and there would be limited increases in the maximum burning rate in the external volume; any escalation in explosion severity to the external volume will likely be caused by the size of the fireball as an ignition source.

On the other hand, for boxes closed by a door there would be jets of high speed unburned gas driven out all around the edge of the widening vent. These jets would generate high levels of turbulence in the larger volume allowing the external flame to extend very rapidly away from the ignited box when it emerges. Overall burning rates in the external volume would be greatly increased which would lead in turn to higher pressures and more energetic outflow if there was another level of nesting – for example a pump house enclosure venting into an engulfing gas cloud.

This analysis suggests that the venting mechanism and flame exit speeds as a result of the door are likely to result in a more severe explosion in the an external volume, compared to a bursting membrane vent. However, it is not currently possible to

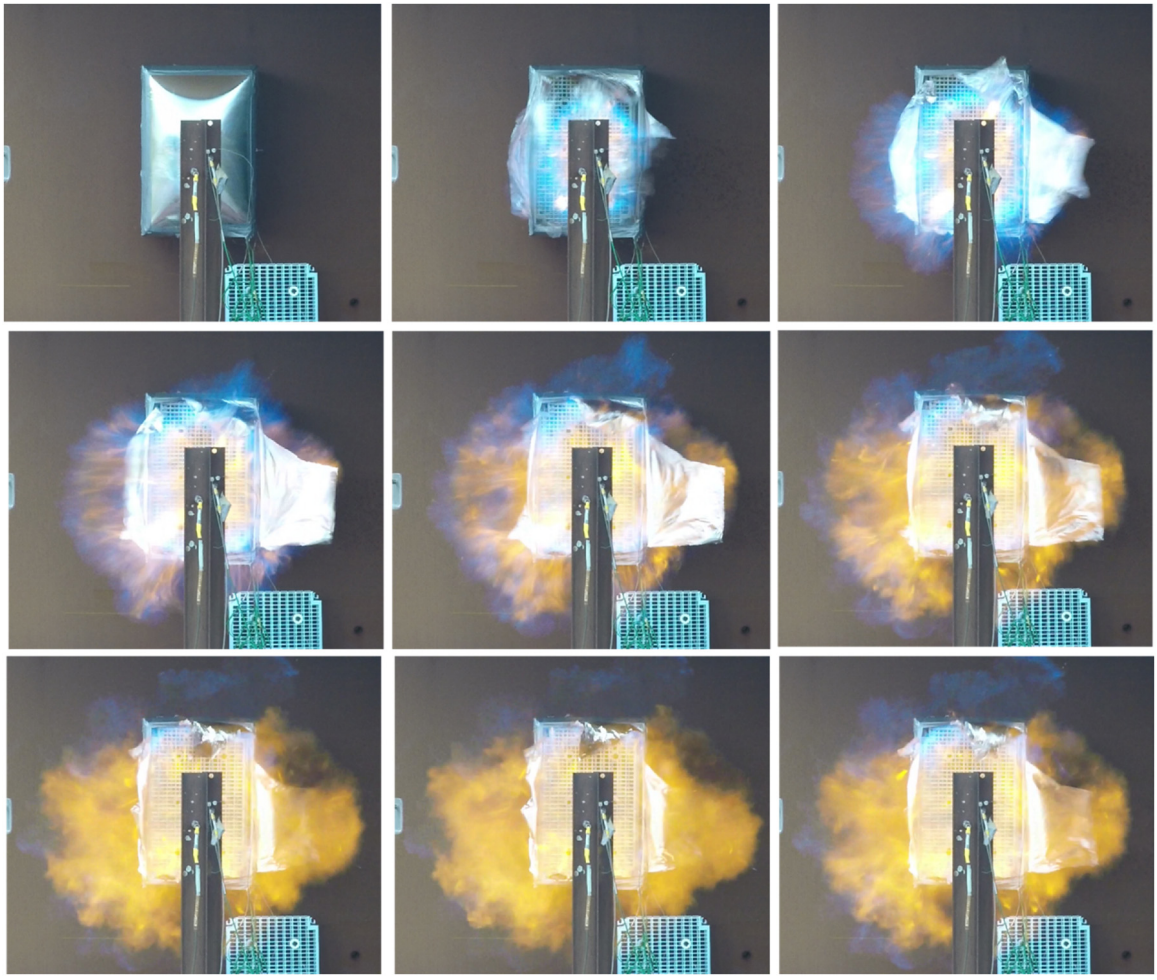

Fig. 26. Test 6 external flame from front - Frame interval 4.17 ms.

fully predict the extent to which these mechanisms will affect the explosion severity in an external unconfined volume. Further work with a flammable atmosphere is planned to investigate this issue.

The work by Daubech et al. (2017) was conducted to explore the same problem as this study and gives a valuable base for the theory. Although the volumes are larger and vents were different than in the experiments described in this paper, the results are of interest. When using an explosion propagating from a 0.7 × 0.7 m vent is used to ignite a larger external volume, a mushroom flame, typical of the vortex bubble is observed. The event does have an escalating effect on the combustion of the unconfined volume. But when the vent was restricted to 0.2 m x 0.2 m the flame was observed as a jet that propagated much further into the unconfined cloud, entraining gas from that volume into the stream and caused a more severe explosion. Note, however, both vents in this study were closed with lightweight membrane and the dynamics of venting were very different to those in this study.

The control box at Buncefield was nested within a steel clad building. In the second stage of the explosion, all the steel cladding panels were simultaneously driven at high speed into the surrounding gas cloud. Previous work (Gill et al., 2016) has shown that panel detachment can also have an escalating effect on the severity of a venting explosion. The process of venting in the early part of the second stage explosion is via the lightweight panels distorting under the rising pressure. Many of these will detach along one side and hinge open before the flame exits. Therefore the flame will be propagating into a cloud that has many areas of turbulence caused by the numerous streams of jetting vented gas.

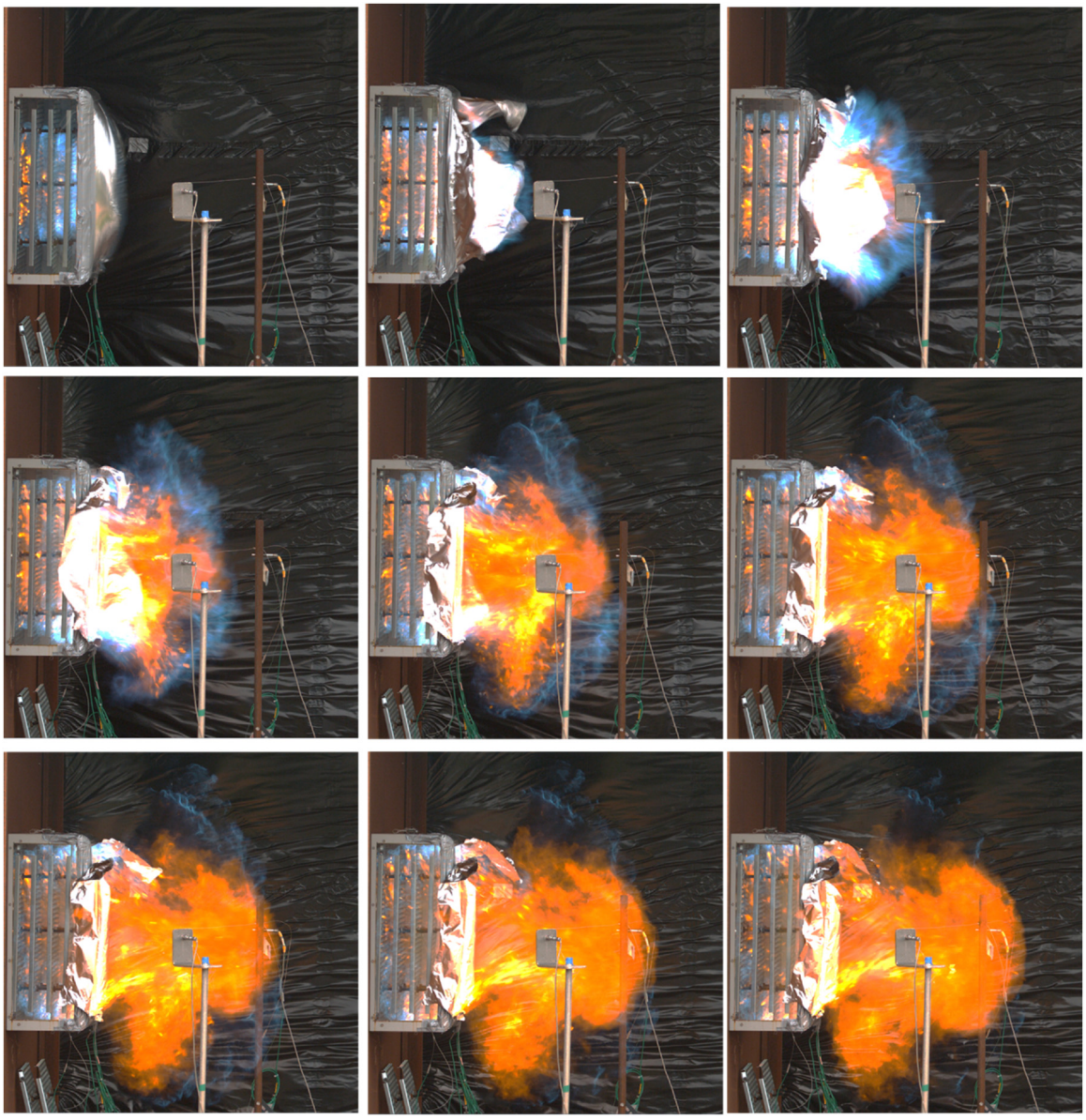

Fig. 27. Test 6 external flame from side - frame interval 4 ms.

The results show that the use of a bursting membrane over a large vent is not appropriate when evaluating the escalating effects of an explosion propagating from an electrical control box (or a larger clad enclosure) either experimentally or through modelling.

Funding

This work was funded by the Health and Safety Executive.

Disclaimer

This paper and the work it describes were funded by the Health and Safety Executive (HSE). Its contents, including any opinions and/or conclusions expressed, are those of the authors alone and do not necessarily reflect HSE policy.

Fig. 28. Test 8 external flame from side - frame interval 4 ms.

Declaration of Competing Interest

The authors declare that they have no known competing financial interests or personal relationships that could have appeared to influence the work reported in this paper.

Appendix A. Supplementary data

Supplementary material related to this article can be found, in the online version, at doi:https://doi.org/10.1016/j.psep.2019.12.026.

References

Atkinson, G., 2006. Buncefield Investigation: Forensic Examination of an Emergency Pumphouse. HSL Report FS/06/11.
Atkinson, G., Coldrick, S., 2012. Vapour Cloud Formation Experiments and Modelling. HSE Research Report RR908.
Atkinson, G., Coldrick, S., Gant, S., Cusco, L., 2015. Flammable vapor cloud generation from overfilling tanks: learning the lessons from Buncefield. J. Loss Prev. Process Ind. 35, 329–338.
Atkinson, G., Cowpe, E., Halliday, J., Painter, D., 2017a. A review of very large vapour cloud explosions: cloud formation and explosion severity. J. Loss Prev. Process Ind. 48, 367–375.
Atkinson, G., Hall, J., McGillivray, A., 2017b. Review of Vapor Cloud Explosion Incidents. HSE Research Report RR1113 2016 (01/09/2016).

Bauwens, C.R., Chaffee, J., Dorofeev, S., 2010. Effect of ignition location, vent size, and obstacles on vented explosion overpressures in propane-air mixtures. Combust. Sci. Technol. 182, 1915–1932.
Bradley, D., Chamberlain, G.A., Drysdale, D.D., 2012. Large vapour cloud explosions, with particular reference to that at Buncefield. Philos. Trans. R. Soc. 370, 544–566.
Briggs, G.A., Thompson, R.S., Snyder, W.H., 1990. Dense gas removal from a valley by crosswinds. J. Hazard. Mater. 24, 1–38.
Burgess, D.S., Zabetakis, M.G., 1973. Detonation of a Flammable Cloud Following a Propane Pipeline Break: the December 9, 1970, Explosion in Port Hudson, Mo.
Coldrick, S., Gant, S.E., Atkinson, G.T., Dakin, R., 2011. Factors affecting vapour production in large scale evaporating liquid cascades. Process. Saf. Environ. Prot. 89 (6), 371–381.
Daubech, J., Proust, C., Lecocq, G., 2017. Propagation of a confined explosion to an external cloud. J. Loss Prev. Process Ind. 49, 805–813.
Fakandu, B.M., Andrews, G.E., Phylaktou, H.N., 2015. Vent burst pressure effects on vented gas explosion reduced pressure. J. Loss Prev. Process Ind. 36, 429–438.
Gill, J., Atkinson, G., Cowpe, E., Painter, D., 2016. Vapour cloud explosions in steel clad structures. Symposium Series No 161, HAZARDS 26 Conference.
Gill, J., Atkinson, G., Phylaktou, H., Andrews, G.E., Cowpe, E., 2019. Explosions in electrical control boxes as a potential “Nested bang-Box” mechanism for severe vapour Cloud. Explosions In Proceedings of Ninth International Seminar on Fire and Explosion Hazards, 356–365.
Harris, R.J., Wickens, M.J., 1989. Understanding Vapour Cloud Explosions - an Experimental Study IGE Comm., pp. 1408.
Major Incident Investigation Board, 2007. The Buncefield Incident – 11th December 2005 – the Final Report of the Major Incident Investigation Board, Vol 1.
Maxworthy, T., 1972. The structure and stability of vortex rings. J. Fluid Mech. 51 (1), 15–32.
Pekalski, A., Puttock, J., Chynoweth, S., 2015. Deflagration to detonation transition in a vapour cloud explosion in open but congested space: large scale test. J. Loss Prev. Process Ind. 36, 365–370.
Proust, C., Leprette, E., 2010. The dynamics of vented gas explosions. Process. Saf. Prog. 29 (3), 231–235.
Tomlin, G., Johnson, D.M., Cronin, P., Phylaktou, H.N., Andrews, G.E., 2015. The effect of vent size and congestion in large-scale vented natural gas/air explosions. J. Loss Prev. Process Ind. 35, 169–181.